



Projecting circum-Arctic excess ground ice melt with a sub-grid representation in the Community Land Model

Lei Cai¹, Hanna Lee¹, Kjetil Schanke Aas², Sebastian Westermann²

¹NORCE Norwegian Research Centre, Bjerknes Centre for Climate Research, 5008, Bergen, Norway

5 ²Department of Geosciences, University of Oslo, Oslo, 0315, Norway

Correspondence to: Lei Cai (leca@norceresearch.no)

Abstract To address the longstanding underrepresentation of the influences of highly variable ground ice content on the trajectory of permafrost conditions simulated in Earth System Models under a warming climate, we implement a sub-grid representation of excess ground ice within permafrost soils using the latest version of the Community Land Model (CLM5). Based on the original CLM5 tiling hierarchy, we duplicate the natural vegetated landunit by building extra tiles for up to three different excess ice conditions for each grid cell. For the same total amount of excess ice, introducing sub-grid variability in excess ice contents leads to different excess ice melting rates at the grid level. In addition, there are impacts on permafrost thermal properties and local hydrology with sub-grid representation. We evaluate this new development at a single-point at the Lena river delta, Siberia, where three sub-regions with distinctively different excess ice conditions are observed. A triple-landunit case accounting for this spatial variability conforms well to previous model studies for the Lena river delta and displays a markedly different dynamics of future excess ice thaw compared to a single-landunit case initialized with average excess ice contents. We prescribed a tiling scheme combined with our sub-grid representation to the global permafrost region using the dataset “Circum-Arctic Map of Permafrost and Ground-Ice Conditions” (Brown et al., 2002). The sub-grid scale excess ice produces significant melting of excess ice under a warming climate and enhances the representation of sub-grid variability of surface subsidence on a global scale. Our model development makes it possible to portray more details on the permafrost degradation trajectory depending on the sub-grid soil thermal regime and excess ice melting. The modeled permafrost degradation with sub-grid excess ice follows the pathway that continuous permafrost transforms into discontinuous permafrost before it disappears, including surface subsidence and talik formation, which are highly permafrost-relevant landscape changes excluded from most land models. Our development of sub-grid representation of excess ice demonstrates a way forward to enhance improve the realism of excess ice melt in global land models, but further developments rely on additional global observational datasets on both the horizontal and vertical distributions of excess ground ice.

1. Introduction

Permafrost soils are often characterized by different types of ground ice that can exceed the pore space (Brown et al. 1997; Zhang et al., 1999). The presence of such “excess” ground ice can alter the permafrost thermal regime and landscape structure. Widespread thawing of permafrost is expected in a warmer future climate and modeling studies suggest large-scale degradation of near-surface permafrost



at the end of the 21st century (Lawrence *et al.* 2008 & 2011). Melting of ground ice due to active layer thickening releases water in the form of surface and/or subsurface runoff, causing surface subsidence and modifying the local hydrological cycle (West and Plug, 2008; Gross *et al.*, 2011; Kokelj *et al.*, 2013; Westermann *et al.*, 2016). In addition to containing ground ice, some permafrost soils store massive
40 amounts of carbon, which could be released to the atmosphere in the form of greenhouse gases upon thawing (Walter *et al.*, 2006; Zimov *et al.*, 2006; Schuur *et al.*, 2008), possibly making a positive feedback to amplify future climate change (Koven *et al.*, 2011; Schaefer *et al.*, 2011; Burke *et al.*, 2013). The existence of excess ice and its distribution in permafrost can significantly affect the rate of permafrost thawing, and in turn, the rate of soil carbon release (Hugelius *et al.*, 2014; Schuur *et al.*, 2015; Turetsky
45 *et al.*, 2019). Therefore, better projections of excess ice melt are critical to improve our understanding of the impacts of permafrost thaw on corresponding climatic impacts.

Previous studies address excess ice modeling on the local or regional scale, in which the small study area makes it possible for detailed configurations of the cryostratigraphy of permafrost and excess ice based on observations. Simulations for the Lena river delta have retrieved the permafrost thermal
50 dynamics fairly close to the observations with excess ice incorporated in the modeling (Westermann *et al.*, 2016). A two-tile approach allowing lateral heat exchange between two land elements demonstrated that maintaining thermokarst ponds requires the heat loss from water to the surrounding land (Langer *et al.*, 2016). A similar tiling approach has been applied to projecting the landscape changes due to permafrost thaw for ice-wedge polygons and peat plateaus with different features of ice melting and
55 surface subsidence (Aas *et al.*, 2019; Nitzbon *et al.*, 2019).

On the global scale, the land components of Earth System Models (ESMs) have significant capabilities of representing key permafrost physics. In the Community Land Model (CLM), for example, the representation of permafrost-associated processes has been continuously improved over generations. By including key thermal and hydrological processes of permafrost, the CLM version 4 (CLM4) has
60 reasonably reproduced the global distribution of permafrost (Lawrence *et al.*, 2008; Lawrence *et al.*, 2012; Slater and Lawrence, 2013). Projections based on the CLM4 under its highest warming scenario (RCP8.5) have shown over 50% degradation of near-surface permafrost by 2100 (Lawrence *et al.*, 2012). Moreover, the recently released CLM5 has more advanced representations of many biogeophysical and biogeochemical processes (Lawrence *et al.*, 2019). A refined soil profile and upgraded snow
65 accumulation and densification scheme in the CLM5 could contribute to simulating more realistic permafrost thermal regimes, whereas upgrades on biogeochemistry improve simulations of soil carbon release in response to permafrost thaw. Separate from this, an excess ice physics scheme has been implemented in CLM4.5 (CLM4.5_EXICE) by Lee *et al.* (2014), which allowed for the first-order simulation of surface subsidence globally by modeling excess ice melt under a warming climate.

70 The homogeneous distribution of excess ice throughout the grid cell in CLM4.5_EXICE (Lee *et al.*, 2014) could cause biases in thaw trajectories in the warming climate. In nature, excess ice forms in a highly localized manner due to a variety of accumulation processes. For instance, segregated ice lenses formed during frost heave differ substantially in morphology from ice wedges formed from repeated frost



75 cracking and freezing of penetrating water. Field measurements illustrate that the depth distribution of
ground ice can vary substantially on the order to 10-50 meters horizontally and 10 meters vertically
(Pascale et al., 2008; Fritz et al., 2011). The horizontal grid spacing of ESMs, on the other hand, usually
ranges from one to two degrees (~100-200km horizontal scale), which makes it impossible to represent
localized excess ice. The mismatch in spatial scale between model and the real world raises concerns for
the reliability of excess ice modeling in ESMs. Aside from the homogenously-initialized excess ice in
80 the grid cell, CLM4.5_EXICE initializes excess ice in the same soil depths globally (below 1m),
regardless of the varying active layer thickness in circum-Arctic permafrost areas (Lee et al., 2014). Such
deficiencies in excess ice parameterization hamper global projections of permafrost thaw including
excess ice with ESMs.

To narrow the gap between the high spatial variability of excess ice and the coarse grid spacing in
85 the ESMs, we applied a sub-grid approach in representing excess ice in permafrost soils within the CLM5
to investigate how presence and melting of excess ice affect land surface physics under a warming climate.
We conducted idealized single-point simulations to examine the robustness of model development. We
furthermore conducted global simulations using a prescribed set of sub-grid scale excess ice conditions,
aiming to bring the modeling of excess ice melt and the corresponding impacts on the global scale
90 towards a higher accuracy.

2. Methodology

2.1 Sub-grid representation of excess ice in the CLM5

The CLM5 model utilizes a three-level tiling hierarchy to represent sub-grid heterogeneity of
landscapes, which are (from top to bottom) landunits, columns, and patches (Olsen et al., 2010). There
95 is only one column (the natural soil column) that is under the natural vegetated landunit, which represents
soil including permafrost. In this study, we modify the CLM5 tiling hierarchy by duplicating the natural
vegetated landunit, making extra landunits for prescribing up to three different excess ice conditions in
permafrost (Figure 1). The original natural vegetated landunit is considered as “natural vegetated with
no excess ice” (hereafter no ice landunit), while we denote the additional landunits as “natural vegetated
100 with low content of excess ice” (hereafter the low ice landunit), “natural vegetated with medium content
of excess ice” (hereafter the mid ice landunit), and “natural vegetated with high content of excess ice”
(hereafter the high ice landunit). The sub-grid initial conditions of excess ice are imported as part of the
surface data, which includes the variables of volumetric excess ice contents, depths of the top and bottom
soil layer of added excess ice, and the area weights of the four landunits.

105 We adopted the excess ice physics from CLM4.5_EXICE (Lee et al., 2014), including
thermodynamic and hydrological processes. The added excess ice is evenly distributed within each soil
layer, which in turn increases soil layer thickness. Because ice density is considered constant, the increase
of soil layer thickness is linearly proportional to the volumetric ice content. The revised algorithm for
thermal conductivity and heat capacity of soil involves the effects of added excess ice, while the revised



110 phase change energy equation allows excess ice to melt. The meltwater adds to soil liquid water in the
same soil layer, and it can move to the above layer if the original layer is saturated. Such numerical
implementation replicates how the melt excess ice eventually converts to runoff and discharges from the
soil in case of well-drained conditions. As excess ice melts, soil layer thickness decreases, which
corresponds to surface subsidence due to excess ice melt. In our model parameterization, excess ice only
115 melts and does not re-form since the applied excess ice physics does not account for the different ice
formation processes.

Aside from sub-grid tiles for excess ice, we acknowledge that the version upgrade from CLM4.5 to
CLM5 as the base model modifies the results of excess ice melt compared to the results from Lee et al.
(2014). By default, CLM5 represents soil with a 25-layer profile, for which the top 20 hydrologically-
120 active layers cover 8.5 meters of soil. There are additional 10 soil layers and it is 4.7 meters deeper
compared to the default hydrologically-active soil layer profile in CLM4.5, not to mention the
substantially more complex biogeophysical processes (Lawrence et al., 2019). Therefore, we developed
the sub-grid representation of excess ice within the framework of the latest version of CLM. The
duplicated landunits prolong computation time by roughly 10% compared to the original CLM5. We are,
125 therefore, confident that our model development is highly efficient in addressing the sub-grid excess ice
and subsequent permafrost thaw.

2.2 Single-point simulations for the Lena river delta, Siberia

We conduct single-point simulations for the Lena River delta and compare the CLM5 model results
to reference simulations with the CryoGrid3 model for the same location (Westermann et al., 2016).
130 Abundant background information is available on the soil and ground ice dynamics from both
observation and modeling, making the Lena river delta a suitable location to further evaluate our model
development. The Lena river delta can be broadly categorized into three different geomorphological units
that have distinctively different subsurface cryostratigraphies of excess ice (Schneider et al., 2009; Ulrich
et al., 2009). In the eastern and central part of the river delta, ground ice has been accumulated in the
135 comparatively warm Holocene climate. The subsurface sediments (hereafter denoted as “Holocene
ground ice terrain”) are generally super-saturated with wedge ice that can extend up to 9 meters
underground with the volumetric ice contents ranging from 60-80% (Schwamborn et al., 2002; Langer
et al., 2013). On the other hand, higher excess ice contents are found in Pleistocene sediments in the Lena
River Delta (hereafter the “Yedoma Ice complex”), which are characterized by Yedoma type round ice
140 (Schirrmeister et al., 2013), which can reach depths of up to 20-25 meters deep and volumetric ice
contents as high as 90% (Schwamborn et al., 2002; Schirrmeister et al., 2003 and 2011). Finally, the
Northwestern part of the delta features sandy sediments and is characterized by low excess ice contents
(hereafter denoted the “no excess ice terrain”; Rachold and Grigoriev, 1999; Schwamborn et al., 2002).

We determine the area weights of excess ice landunits in one single point based on the spatial pattern
145 of three subregions (Fedorova et al., 2015). The cryostratigraphy and ice content of excess ice strictly
follow those in Westermann et al. (2016). Meanwhile, we did not customize soil properties for different
landunits as in Westermann et al. (2016), as our model development does not support varying soil



properties for different sub-grid landunits. We also directly apply the snow accumulation physics in the CLM rather than customizing the snow density. By default, the current model does not form thermokarst lakes as the meltwater from excess ice melt becomes surface runoff and is removed from the grid cell. To apply the sub-grid representation, we initialize the case with three landunits (the triple-landunit case) that respectively represent the three terraces in the Lena river delta. We also initialize an “average ice single-landunit” case without the sub-grid representation of excess ice. The excess ice amount for each soil layer in the average ice single-landunit case is initially the same as that in the triple-landunit case. The volumetric ice content is determined by spatial averaging those for three excess ice landunits in the triple-landunit case. Detailed information on the applied excess ice conditions for both cases is listed in Table 1.

We employed the single-point forcing data from in Westermann et al. (2016) for the Lena river delta from 1901 to 2100, which is based on the CRU-NCEP (<http://dods.extra.cea.fr/data/p529viov/cruncep/>) data set for the historical period (1901-2005) and the CCSM4 model output under the RCP4.5 scenario for the projected period (2006-2100), but downscaled with in-situ observations. We run 100-year spin-up simulations in order to stabilize the permafrost thermal regime after adding excess ice. Spin-up simulations are produced by running the model with cycled 1901-1920 climatological data. The purpose of spin-up simulations is to stabilize ground temperatures and excess ice contents. The 100-year length for spin-up is sufficient, as the model is run in Satellite Phenology (SP) mode that does not involve slowly evolving biogeochemical processes such as soil carbon accumulation. Moreover, we address idealized single-point simulations for additional permafrost locations with both continental and maritime climate that showcase the difference to Lee et al. (2014), the results of which are included in the Supplementary material.

2.3 Global simulations of excess ice melt using sub-grid initialization

The information available for the spatial distribution and cryostratigraphy of excess ice on the global scale is generally not as detailed as in the Lena river delta due to the lack of observations. For our global simulations we employ the widely used “Circum-Arctic Map of Permafrost and Ground-Ice Conditions” (hereafter the CAPS data; Brown et al., 2002) as data source, while we translate the ground ice condition in the CAPS data to different excess ice stratigraphies as model input data. The CAPS permafrost map categorizes the global permafrost area into classes coded by three factors (i) permafrost extent (c = continuous, d = discontinuous, s = sporadic, and i = isolated), (ii) visible ground ice content (h = high, m = medium, and l = low), and (iii) terrain and overburden (f = lowlands, highlands, and intra- and intermontane depressions characterized by thick overburden cover, and r = mountains, highlands ridges, and plateaus characterized by thin overburden cover and exposed bedrock), resulting in more than 20 different varieties in permafrost characteristics (Figure 2). For the simulations, we only use the CAPS distinction between the three classes high, medium and low ice contents. We qualitatively categorize excess ice types with typical cryostratigraphies for which observations are available, recognizing that this is a crude first-guess of the global distribution of ground ice.



185 The high ice CAPS classes (e.g. chf, chr, and dhf) in central and eastern Siberia, as well as in Alaska,
partly coincide with Yedoma regions (Kanevskiy et al., 2011; Grosse et al., 2013). The cryostratigraphy
of the high ice landunit is therefore broadly oriented at the excess ice contents and distribution in intact
Yedoma, which is characterized by massive ice wedges leading to typical average volumetric ice contents
190 in the range from 60% to 90% (Schwamborn et al., 2002; Kanevskiy et al., 2011). We therefore set the
volumetric excess ice content to 70%, and we put excess ice in all the soil layers between 0.2 meters
below the active layer and the bottom of hydrologically-active soil layer (8.5 meters). The onset depth of
the excess ice just below the active layer is based on the assumption of active ice aggradation which
occurs at or below the permafrost table, e.g. the formation of wedge or segregation ice. For the low ice
landunit, we assume both a significantly lower volumetric ice content and a smaller vertical extent of the
195 excess ice body. The volumetric excess ice content is set to 25%, and we add excess ice at soil layers
within 0.2 to 1.2 meters below the active layer, which in particular represents sediments with segregated
ice (e.g. Cable et al., 2018), but also accounts for a wide range of different excess ice conditions found
throughout the permafrost domain. For the mid ice landunit, we set the ice content as 45% and put excess
ice within 0.2 to 2.2 meters below the active layer, making the volumetric ice content and vertical extent
200 of which in between those for the low and high ice landunits. The cryostratigraphies determine that excess
ice melt in the low ice landunit can result in maximum of 0.36 meters of surface subsidence, while excess
ice melt in the medium ice landunit can result in a maximum of 1.78 m of surface subsidence. For the
high ice landunit, the surface subsidence can be more than 10 meters if all excess ice melts, which is
expected to vary in space because of the different active layer thickness. It is also quite unlikely for all
205 the excess ice in the high ice landunit to melt away by the end of 21st century, so the resulted surface
subsidence could be substantially smaller than 10 meters. For all three landunits, the active layer
thickness is determined by the soil temperature profile by the end of the spinup in a no ice case, which is
the simulation by the original CLM5 model without excess ice incorporated. Non-permafrost regions in
the CAPS data are assigned the no ice landunit for 100% of their area. We emphasize that the prescribed
210 cryostratigraphies are a coarse first-order approximation that can by no means represent the wide variety
of true ground ice conditions found in the permafrost domain. Nevertheless, this makes it possible to
gauge the effect of excess ice melt on future projections of the permafrost thermal regime, when
compared to “traditional” reference simulations without excess ice.

215 We design a tiling scheme prescribing the assignment of landunits for each CAPS class based on
previous observations and empirical estimates (Table 2). All CAPS classes in this study are categorized
into three levels volumetric ice content (5%, 15%, and 25%) that are converted from the ranges (<10%,
10-20%, and >20%) in the original CAPS data. The goal of our tiling scheme is to determine a
combination of area weights of three excess ice landunits for each CAPS class, making the spatially
averaged volumetric ice content the same as that for the CAPS class. We assume that all CAPS classes
220 have the same area fraction of the low ice landunit, and the CAPS classes with a higher ice content are
due to the existence of the landunits with a higher content excess ice. The assumption is based on that
the segregated ice is widely distributed in the permafrost (Miller, 1972; Calmels and Allard, 2008). Given
the ice content prescribed above, all CAPS classes are assigned 20% area of low ice landunit.
Correspondingly, the CAPS classes with 15% volumetric ice content are assigned another 14% area



225 weight for mid ice landunit on top of the CAPS classes with 5% volumetric ice content, while the CAPS
classes with 25% volumetric ice are assigned another 22% area for high ice landunit on top of the CAPS
classes with 15% volumetric ice content. The classes of “chf” and “chr” are the exceptions as their
corresponding regions are typically with the landscape of Yedoma and/or ice wedge polygonal tundra
(Kanevskiy et al., 2011; Gross et al., 2013). We therefore assign only the low and high ice landunits for
230 these two CAPS classes. Summing up the landunit fractions for all the CAPS grid cells within each CLM
grid cell obtains the area weights on the grid level that are stored in the surface data file. Figure 3 shows
a schematic plot for the initialization scenario and the area covered by different excess ice landunits as
the result of sub-grid excess ice initialization in the global simulation case. Note that excess ice for some
regions (e.g. Southern Norway and the Alps) can completely melt out during the spinup period since the
235 CLM initial condition prescribes overly warm (non-permafrost) soil temperature for these regions.

In this study, we define the grid cells/landunits with permafrost as the ones having at least one
hydrologically active soil layer that has been frozen in the last consecutive 24 months. In this case, we
define degraded permafrost as permafrost landunits with an active layer thickness of more than 6.5 meters.
We also prepare a “grid-average ice case” by applying the same total amount of excess ice as in the sub-
240 grid ice case in each soil layer, but using only one landunit instead of three that account for the sub-grid
variability of excess ice. The volumetric ice content in the single landunit is calculated as the spatial
average of those in the three landunits in the triple-landunit case. This grid-average ice case provides a
reference to evaluate the effects of the sub-grid excess ice representation on the global scale. Finally, we
simulate a reference case without excess ice, denoted the “no ice case” in the following. Details on the
245 three cases for the global simulations are listed in Table 3. All global cases are forced by the 3rd version
of Global Soil Wetness Project forcing data (GSWP3; Kim et al., 2012), running in the Satellite
Phenology (SP) mode. The International Land Atmosphere Model Benchmarking (ILAMB; Collier et
al., 2018) project has indicated the superior performance of GSWP3 data forcing the CLM5 in the SP-
only mode
250 ([http://webext.cgd.ucar.edu/I20TR/_build_090817_CLM50SPONLY_CRUNCEP_GSWP3_WFDEI/in
dex.html](http://webext.cgd.ucar.edu/I20TR/_build_090817_CLM50SPONLY_CRUNCEP_GSWP3_WFDEI/index.html)). We conducted a 100-year spin-up using the 1901-1920 climatology before conducting
historical period simulations covering 1901-2005. The anomaly forcing under the RCP8.5 scenario on
top of the 1982-2005 climatology forces simulations in the projected period.

3. Result

255 3.1 Excess ice melt simulations for Lena River delta cryostratigraphies

By the end of the spinup in the triple-landunit case, the active layer thickness is 0.85 m, 0.55 m, and
0.45 m for the ice-poor terrain, the Holocene ice wedge terrain, and the Yedoma ice complex, respectively.
On the other hand, the active layer thickness for the average ice single-landunit case is 0.85 m, which is
the same as in the no excess ice terrain in the triple-landunit case. A small amount of excess ice (24kg/m²)
260 melts during the spinup period, resulting in 2.6 cm surface subsidence throughout the grid.



For the Yedoma ice complex, very little excess ice melt in the 1950s, and it stabilizes afterwards until the late 2000s when substantial ice melt and surface subsidence starts to happen. For the Holocene ground ice terrain, there is no excess ice melt before the late 2010s. By the year 2100, the Yedoma ice complex has exhibited nearly 4 meters of surface subsidence, while the Holocene ground ice terrain has about 0.6 meters of surface subsidence (Figure 4). For the average ice single-landunit case, the noticeable excess ice melt and surface subsidence starts in the late 2010s, which creates about 0.5 meters of surface subsidence by 2100. The magnitude of surface subsidence in the average ice single-landunit case is lower than both the Holocene ground ice terrain and the Yedoma ice complex in the triple-landunit case.

On the grid scale, the total excess ice melt is higher in the average ice single-landunit case than in the triple-landunit case (Figure 5). By the year 2100, the average ice single-landunit case has about 30 kg/m² more excess ice melt than the triple-landunit case. The difference in excess ice on the grid level results from the different volumetric ice content caused by the spatial averaging. In this way, the sub-grid representation of excess ice can potentially also provide more detailed and realistic representation of model variables on the grid level. This is particularly important for the CLM5, which serves as the land component in Earth System Models, which requires the coupling between interacting components on the grid level.

Compared to Westermann et al. (2016), the CLM5 with sub-grid excess ice simulates slightly less (~ 20% less) surface subsidence by 2100 for both the central delta and ice complex. We consider it as a good agreement as we do not expect a closer fit of the model results due to substantial differences in the model physics (for example, the Cryogrid3 simulations in Westermann et al. (2016) lack a representation of the subsurface water cycle). What is in common between these two studies is the earlier start of excess ice melt and more surface subsidence in the ice complex than in the central delta. The CLM5 with sub-grid excess ice also exhibits the varying active layer thickness with different excess ice conditions as Cryogrid3. These results suggest that the new model development enables small-scale variability in excess ice melt and subsequent impacts in agreement with previously published modeling efforts.

3.2 Global projection of permafrost thaw and excess ice melt

Single-point simulations have shown that the varying excess ice cryostratigraphies for different landunits result in sub-grid variabilities of excess ice melt and surface subsidence under the warming climate. The same features remain in the sub-grid ice case within the global simulations that excess ice in the low ice landunit can completely melt out throughout the circum-Arctic permafrost region by the end of the 21st century (Figure 6). The modeled magnitude of surface subsidence is similar to the ~10 cm surface subsidence observed in Barrow and West Dock in the early 21st century (Shiklomanov et al., 2013; Streleskiy et al., 2017). The magnitude of surface subsidence is also comparable to the 1-4 cm decade⁻¹ surface subsidence rate on average over the North Slope of Alaska observed by satellite measurements since the 1990s (Liu et al., 2010). In comparison, the absence of surface subsidence for Arctic Alaska modeled by Lee et al. (2014) is due to an overly deep (1 m deep) excess ice initialization depth. By the year 2100, most ice in the medium ice landunit melts away in the sub-arctic region, while there is less ice melt in the colder regions such as the North Slope of Alaska and the central Siberia. The



high ice landunit has the greatest surface subsidence among the three because of its high ice content,
300 leading to 2-5 meters of surface subsidence by the year 2100.

The existence of excess ice modulates the thermal regime of permafrost soil and is a major control
on permafrost degradation trajectories in a warming climate. We define the permafrost degradation in
this study as when all the landunits in one grid cell has an active layer thickness greater than 6.5 meters.
Permafrost with excess ice consistently exhibits delayed permafrost degradation compared to the no ice
305 case (Figure 7). For the no ice case modeled by the original CLM5, more than half of the permafrost area
undergoes degradation by the end of the 21st century. By 2100, the only areas where permafrost remains
are the North Slope of Alaska, Northern Canada, and the majority of the land area in the Northern Siberia.
The areas with remaining permafrost in the year 2100 under the RCP8.5 scenarios are substantially larger
compared to the CLM4 simulations, in which nearly all permafrost in Eurasia becomes degraded
310 (Lawrence et al., 2012). For the grid-average ice case, the presence of excess ice stabilizes the permafrost
thermal regime, thus sustains larger permafrost areas on a global scale in the simulation. For example,
permafrost areas in some subarctic regions in the eastern and western Siberia, as well as part of the Arctic
coastal regions in Yukon Territory, Canada, remain in the grid ice case by 2100. Compared to the grid-
average ice case, even more permafrost areas are sustained in the sub-grid ice case, most of which are
315 located in southern Siberia. In the subarctic regions in Alaska and Northwest Canada as well as part of
the central Siberia, permafrost degradation is delayed from the 2040s in the grid ice case to the 2080s in
the sub-grid ice case. We emphasize that permafrost is only sustained according to the accepted
temperature-based definition (ground material at temperature below zero for two consecutive years), but
excess ice continuously melts in this process, which energetically is a different mode of permafrost
320 degradation, similar to a negative mass balance of glaciers and ice sheets.

In the sub-grid ice case, the landunits with high ice contents lead to more grid points for which
permafrost conditions remain in the year 2100 compared to the grid-average ice case. On the other hand,
permafrost with excess ice only covers a fraction of a grid point. Among the permafrost degradation
trajectories in the three global simulation cases (Figure 8), the sub-grid ice case can provide a more
325 detailed picture on the timing of permafrost degradation. Grid cells become ‘partially degraded
permafrost’ if landunits with excess ice still contain permafrost, which phenomenologically is a more
realistic representation that also makes it possible to represent the permafrost distribution in the
discontinuous and sporadic permafrost zones. On the other hand, only “fully degraded permafrost” and
“remaining permafrost” can be distinguished for the no ice and grid-average ice case. Under the warming
330 climate in the 21st century, the existence of excess ice, especially the high content excess ice, has a
stabilizing effect on soil temperature that delay the disappearance of permafrost on the sub-grid level.
Therefore, by the year 2100, there are regions with partially degraded permafrost in between intact and
degraded permafrost (Figure 8). For example in western Siberia, the Pacific coastal area of eastern
Siberia, Northwestern Canada, and along the Brooks Range in Alaska, taliks form for landunits with low
335 ice contents which leads to partially degraded permafrost regions. Therefore, permafrost degradation
exhibits a gradual transition from continuous to discontinuous permafrost, and to non-permafrost regions.



Some of these regions also encounter substantial surface subsidence in the high ice landunit (> 5 m) (Figure 6).

We further compare the total permafrost area (defined as landunits with active layer thickness < 6.5 meters) in the three cases throughout time. The differences in permafrost area increase from the grid-average ice case and sub-grid ice case to the no ice case at a rate of 1000 km² per year until 2050 (Figure 9). After 2050, the area difference of permafrost in the grid-average ice case and no ice cases rapidly increases, which reaches nearly one million km² by 2100. In the sub-grid ice case, the rate of increase remains relatively unchanged after 2050, resulting in an about 0.2 million km² larger permafrost area than that in the no ice case.

4. Discussion

The aim of the sub-grid excess ice representation in the CLM5 is to facilitate long-term global projection of excess ice melt and surface subsidence in the permafrost regions, but the corresponding observational data for model evaluation is sparse, considering especially that drastic excess ice melt as projected until 2100 is only observed in few locations today (e.g. Günther et al., 2015). In the following, we discuss the challenges and limitations of the sub-grid excess ice framework, and how this sub-grid representation can potentially help the development of other CLM components.

Both single-point and global test simulations in this study have shown that excess ice melts under a warming climate is sensitive to its initialization depth. The active-layer-dependent excess ice initialization in this study in the global simulation (sub-grid excess ice case) yields excess ice melt and surface subsidence rates in the early 2000s that are comparable to observations. The lower depths of the assumed excess ice body controls the termination of excess ice melt which at the same time determines the onset of talik formation in many permafrost areas. Due to the scarcity of observational data, it is unclear to what extent the cryostratigraphies assumed in our tiling scheme can reproduce the true vertical extent of excess ice bodies at least in a statistical sense. Even so, we manage to make the prescribed excess ice condition as close to the previous results as possible. Firstly, our tiling scheme on the large scale strictly follows the CAPS data (Brown et al., 2002) in terms of the volumetric excess ice content. Furthermore, statistics by Zhang et al. (2000) suggest the ranges of the vertical extent of ice-rich permafrost of 0-2 meters and 2-4 meters respectively for the CAPS classes with low (5%) and medium (15%) ice content. Comparatively, the vertical extents permafrost with excess ice prescribed by our tiling scheme are respectively 1.36 meters and 3.78 meters for the same CAPS classes, both of which lie within the ranges in Zhang et al. (2000). The vertical extent of ice-rich permafrost for the high ice landunit is much higher than that (4-6 meters) in Zhang et al. (2000), but the unmelted part of the ice bodies does not strongly affect the overall rate of excess ice melt, although the remaining ice can slightly change soil temperature and moisture of the surrounding permafrost. We therefore imply that our high ice landunit initialization would not induce a strong bias in excess ice melt projection in the 21st century.

The tiling scheme ignores possible variations of ice content with soil depth, initializing excess ice as “cubes” with a homogeneous ice content. We simplify the ice content initialization for two reasons.



375 Firstly, the model development serves the land component of an earth system model that focuses on
large-scale changes. Furthermore, there is not enough observational evidence for us to prescribe the
variability of excess ice content with geographic locations and soil depths.

380 Due to such shortcomings in the excess ice initialization, we do not expect the modeled excess ice
melt in this study to be an adequate representation of reality yet, but improved observational data sets of
excess ice contents and cryostratigraphies could be directly ingested to yield improved results. Our model
development is capable of supporting three different excess ice landunits for each grid point, but the
cryostratigraphies assumed in the initialization in principle also vary in space. However, at present, a
spatially distributed global dataset with quantitative information on ice content stratigraphies does not
exist. We emphasize that for a better projection of excess ice melt, more observational data of excess ice
distribution and surface subsidence is required to further evaluate and validate the new model
385 implementation of excess ice. On the regional scale, Jorgenson et al. (2008) presented a permafrost map
of total ground ice volume for the uppermost 5 meters of permafrost based on both observations and
estimates for Alaska. In addition, O'Neill et al. (2019) compiled permafrost maps for Northern Canada
by paleographic modeling, mapping the abundances of three types of excess ice respectively. Further
improvements of model results are dependent of additional observationally constrained datasets of excess
390 ice contents and conditions on the global scale.

The area weights of the excess ice landunits (Table 2) in the global simulation are obtained from the
higher-resolution CAPS points located within a CLM grid cell. However, complex landscape
development, such as thermokarst ponds, requires knowledge of the meter-scale distribution, for example
the extent and geometry of individual ice wedges (Langer et al., 2016; Nitzbon et al., 2019), which cannot
395 be represented with the still coarse-scale excess ice classes from the CAPS map. One possible solution
to represent this could be to include another layer of sub-grid tiles below the CLM landunit level, where
the individual tiles can interact laterally. This would allow for the representation of small-scale
permafrost features within a large-scale landunit with a given excess ice content. An example of how this
could work is given by Aas et al. (2019) who simulated both polygonal tundra and peat plateaus with a
400 two-tile interactive setup. This is also similar to the recent representation of hillslope hydrology by
Swenson et al. (2019), where sub-grid tiles (on the column level in CLM) were used to represent different
elements in a representative hillslope. In the future development of CLM, this could be part of a more
generic tiling system where lateral heat and mass fluxes could be switched on and off to represent a wide
range of land surface processes that are currently ignored or parameterized in LSMs. Fisher and Koven
405 (2020) have discussed the challenges and opportunities in such an adaptive and generic tiling system.
We would also advocate for enhancing current tiling schemes in such a direction, which could
substantially improve the realism in the representation of permafrost landscapes in LSMs. However, the
success of such tiling approach will rely heavily on the availability of adequate observational data, further
highlighting the need for observational efforts and close collaboration between field scientists and
410 modelers.



The more detailed simulation of permafrost degradation trajectory with a sub-grid representation of excess ice also builds more potential on better modelling the permafrost-carbon feedback with biogeochemistry activated (CLM5BGC). Excess ice stabilizes the permafrost thermal regime, therefore alter the rate of carbon releasing from the permafrost (Shuur et al., 2008). Improved projections of permafrost warming could also enhance modelling of vegetation type changes (e.g. shrub expansion) that determines the nitrogen uptake to the atmosphere (Loranty and Goetz, 2012). On the other hand, the possibility to simulate surface subsidence and excess ice meltwater formation also opens the possibility of a more accurate representation of wetland formation. The increase in the area of wetland and soil moisture have an impact of the balance of CH₄ and CO₂ releasing from the permafrost as more organic matter could decompose in an anaerobic pathway (Lawrence et al., 2015; Treat et al., 2015). Compared to the parameterized inundated area simulation in the CLM5 (Ekici et al., 2019), a process-based wetland physics scheme together with the sub-grid representation of excess ice in this study would substantially contribute to the biogeochemical modeling over the circum-arctic area.

5. Conclusion

This study develops a sub-grid representation of excess ice in the CLM5 and examines the impacts of the existence and melting of excess ice in the sub-grid scale in a warming climate. Extra landunits duplicated from the natural vegetated landunit in the CLM sub-grid hierarchy make it possible to prescribe up to three different excess ice conditions in each grid point with permafrost.

A test over the Lena river delta showcases that the sub-grid representation of excess ice can retrieve the sub-grid variability of annual thaw-freeze state and the excess ice melt/surface subsidence through time. On the other hand, initializing excess ice homogenously throughout the grid cell produces a smaller stabilization effect of excess ice to the permafrost thermal regime and the local surface subsidence under warming climate. With a tiling scheme ingesting a global data set of excess ice condition into the CLM surface data, our model development shows the capability of portraying more details on simulating permafrost degradation trajectories. As excess ice thermally stabilizes the permafrost on the sub-grid scale, permafrost degrades with a trajectory from continuous permafrost to discontinuous permafrost, and finally to a permafrost-free area. The modelled global pattern of permafrost therefore exhibits regions of discontinuous permafrost as the transition zone between the continuous permafrost and degraded permafrost.

This study, for the first time, used an ESM to project excess ice melt/surface subsidence and permafrost degradation with sub-grid variability. The approach of duplicating tiles at the landunit level instead of the column level allows more freedom for further developments in this direction. Furthermore, the new CLM tiling hierarchy has much more potential than representing more accurate excess ice physics as examined in this study. Further advancing the excess ice modeling relies on additional observational studies/datasets of the excess ground ice conditions on a global scale. The model development in our study, therefore, lays the foundation for further advances focusing on excess ice



modeling and other processes in the CLM framework that could benefit from an improved sub-grid representation.

450 **Code/Data Availability**

The original Community Land Model is available at <https://github.com/ESCOMP/ctsm>. The source code of model development in this study is available from the corresponding author upon request.

Author contributions

L.C conducted model development work and wrote the initial draft with additional contributions from
455 all authors. H.L, S.W, and K.S.A provided ideas and help during the process of model development. H.L
provided the code of excess ice physics in the earlier version of CLM. L.C prepared all figures.

Acknowledgments

This study is funded by the Research Council of Norway KLIMAFORSK program (PERMANOR;
RCN#255331). We thank Sarah Chadburn for helpful comments and suggestions in preparing this
460 manuscript.

Reference

- Aas, K. S., Martin, L., Nitzbon, J., Langer, M., Boike, J., Lee, H., Berntsen, T. K., and Westermann, S.:
Thaw processes in ice-rich permafrost landscapes represented with laterally coupled tiles in a
465 land surface model, *The Cryosphere*, 13, 591-609, 10.5194/tc-13-591-2019, 2019.
- Brown, J., Ferrians Jr, O., Heginbottom, J., and Melnikov, E.: Circum-Arctic map of permafrost and
ground-ice conditions, US Geological Survey Reston, VA, 1997.
- Burke, E. J., Dankers, R., Jones, C. D., and Wiltshire, A. J.: A retrospective analysis of pan Arctic
permafrost using the JULES land surface model, *Climate Dynamics*, 41, 1025-1038,
470 10.1007/s00382-012-1648-x, 2013.
- Cable, S., Elberling, B., and Kroon, A.: Holocene permafrost history and cryostratigraphy in the High-
Arctic Adventdalen Valley, central Svalbard, *Boreas*, 47, 423-442, 10.1111/bor.12286, 2018.
- Calmels, F., and Allard, M.: Segregated ice structures in various heaved permafrost landforms through
CT Scan, *Earth Surface Processes and Landforms*, 33, 209-225, 10.1002/esp.1538, 2008.
- 475 Collier, N., Hoffman, F. M., Lawrence, D. M., Keppel-Aleks, G., Koven, C. D., Riley, W. J., Mu, M.,
and Randerson, J. T.: The International Land Model Benchmarking (ILAMB) system: design,
theory, and implementation, *Journal of Advances in Modeling Earth Systems*, 10, 2731-2754,
2018.



- 480 Ekici, A., Lee, H., Lawrence, D. M., Swenson, S. C., and Prigent, C.: Ground subsidence effects on
simulating dynamic high-latitude surface inundation under permafrost thaw using CLM5,
Geosci. Model Dev., 12, 5291-5300, 10.5194/gmd-12-5291-2019, 2019.
- Fedorova, I., Chetverova, A., Bolshiyarov, D., Makarov, A., Boike, J., Heim, B., Morgenstern, A.,
Overduin, P. P., Wegner, C., Kashina, V., Eulenburg, A., Dobrotina, E., and Sidorina, I.: Lena
485 Delta hydrology and geochemistry: long-term hydrological data and recent field observations,
Biogeosciences, 12, 345-363, 10.5194/bg-12-345-2015, 2015.
- Fisher, R. A., and Koven, C. D.: Perspectives on the future of Land Surface Models and the challenges
of representing complex terrestrial systems, Journal of Advances in Modeling Earth Systems,
n/a, 10.1029/2018MS001453, 2020.
- 490 Fritz, M., Wetterich, S., Meyer, H., Schirrmeister, L., Lantuit, H., and Pollard, W. H.: Origin and
characteristics of massive ground ice on Herschel Island (western Canadian Arctic) as revealed
by stable water isotope and Hydrochemical signatures, Permafrost and Periglacial Processes, 22,
26-38, 10.1002/ppp.714, 2011.
- Grosse, G., Robinson, J. E., Bryant, R., Taylor, M. D., Harper, W., DeMasi, A., Kyker-Snowman, E.,
Veremeeva, A., Schirrmeister, L., and Harden, J.: Distribution of late Pleistocene ice-rich
495 syngenetic permafrost of the Yedoma Suite in east and central Siberia, Russia, US Geological
Survey Open File Report, 2013, 1-37, 2013.
- Günther, F., Overduin, P. P., Yakshina, I. A., Opel, T., Baranskaya, A. V., and Grigoriev, M. N.:
Observing Muostakh disappear: permafrost thaw subsidence and erosion of a ground-ice-rich
island in response to arctic summer warming and sea ice reduction, The Cryosphere, 9, 151-178,
500 10.5194/tc-9-151-2015, 2015.
- Hugelius, G., Strauss, J., Zubrzycki, S., Harden, J. W., Schuur, E. A. G., Ping, C. L., Schirrmeister, L.,
Grosse, G., Michaelson, G. J., Koven, C. D., O'Donnell, J. A., Elberling, B., Mishra, U., Camill,
P., Yu, Z., Palmtag, J., and Kuhry, P.: Estimated stocks of circumpolar permafrost carbon with
quantified uncertainty ranges and identified data gaps, Biogeosciences, 11, 6573-6593,
505 10.5194/bg-11-6573-2014, 2014.
- Kanevskiy, M., Shur, Y., Fortier, D., Jorgenson, M. T., and Stephani, E.: Cryostratigraphy of late
Pleistocene syngenetic permafrost (yedoma) in northern Alaska, Itkillik River exposure,
Quaternary Research, 75, 584-596, 10.1016/j.yqres.2010.12.003, 2011.
- Kim, H., Yoshimura, K., Chang, E., Famiglietti, J., and Oki, T.: Century long observation constrained
510 global dynamic downscaling and hydrologic implication, AGU Fall Meeting Abstracts, 2012.
- Kokelj, S. V., Lacelle, D., Lantz, T. C., Tunnicliffe, J., Malone, L., Clark, I. D., and Chin, K. S.: Thawing
of massive ground ice in mega slumps drives increases in stream sediment and solute flux across
a range of watershed scales, Journal of Geophysical Research: Earth Surface, 118, 681-692,
10.1002/jgrf.20063, 2013.



- 515 Koven, C. D., Ringeval, B., Friedlingstein, P., Ciais, P., Cadule, P., Khvorostyanov, D., Krinner, G., and Tarnocai, C.: Permafrost carbon-climate feedbacks accelerate global warming, *Proceedings of the National Academy of Sciences*, 108, 14769-14774, 2011.
- Langer, M., Westermann, S., Boike, J., Kirillin, G., Grosse, G., Peng, S., and Krinner, G.: Rapid degradation of permafrost underneath waterbodies in tundra landscapes—toward a
520 representation of thermokarst in land surface models, *Journal of Geophysical Research: Earth Surface*, 121, 2446-2470, 2016.
- Langer, M., Westermann, S., Heikenfeld, M., Dorn, W., and Boike, J.: Satellite-based modeling of permafrost temperatures in a tundra lowland landscape, *Remote Sensing of Environment*, 135, 12-24, <https://doi.org/10.1016/j.rse.2013.03.011>, 2013.
- 525 Lawrence, D. M., Slater, A. G., Romanovsky, V. E., and Nicolsky, D. J.: Sensitivity of a model projection of near-surface permafrost degradation to soil column depth and representation of soil organic matter, *Journal of Geophysical Research: Earth Surface*, 113, 10.1029/2007JF000883, 2008.
- Lawrence, D. M., Oleson, K. W., Flanner, M. G., Thornton, P. E., Swenson, S. C., Lawrence, P. J., Zeng, X., Yang, Z. L., Levis, S., and Sakaguchi, K.: Parameterization improvements and functional
530 and structural advances in version 4 of the Community Land Model, *Journal of Advances in Modeling Earth Systems*, 3, 2011.
- Lawrence, D. M., Koven, C. D., Swenson, S. C., Riley, W. J., and Slater, A. G.: Permafrost thaw and resulting soil moisture changes regulate projected high-latitude CO₂ and CH₄ emissions, *Environmental Research Letters*, 10, 094011, 10.1088/1748-9326/10/9/094011, 2015.
- 535 Lee, H., Swenson, S. C., Slater, A. G., and Lawrence, D. M.: Effects of excess ground ice on projections of permafrost in a warming climate, *Environmental Research Letters*, 9, 124006, 2014.
- Liu, L., Zhang, T., and Wahr, J.: InSAR measurements of surface deformation over permafrost on the North Slope of Alaska, *Journal of Geophysical Research: Earth Surface*, 115, 10.1029/2009j001547, 2010.
- 540 Lorant, M. M., and Goetz, S. J.: Shrub expansion and climate feedbacks in Arctic tundra, *Environmental Research Letters*, 7, 011005, 10.1088/1748-9326/7/1/011005, 2012.
- Miller, R.: Freezing and heaving of saturated and unsaturated soils, *Highway Research Record*, 393, 1-11, 1972.
- Nitzbon, J., Langer, M., Westermann, S., Martin, L., Aas, K. S., and Boike, J.: Pathways of ice-wedge
545 degradation in polygonal tundra under different hydrological conditions, *The Cryosphere*, 13, 1089-1123, 10.5194/tc-13-1089-2019, 2019.
- O'Neill, H. B., Wolfe, S. A., and Duchesne, C.: New ground ice maps for Canada using a paleogeographic modelling approach, *The Cryosphere*, 13, 753-773, 10.5194/tc-13-753-2019, 2019.
- Rachold, V., and Grigoriev, M.: Russian-German Cooperation SYSTEM LAPTEV SEA 2000: The Lena
550 Delta 1998 Expedition, *Berichte zur Polarforschung (Reports on Polar Research)*, 315, 1999.



- Schirrneister, L., Grosse, G., Schwamborn, G., Andreev, A. A., Meyer, H., Kunitsky, V. V., Kuznetsova, T. V., Dorozhkina, M. V., Pavlova, E. Y., Bobrov, A. A., and Oezen, D.: Late Quaternary History of the Accumulation Plain North of the Chekanovsky Ridge (Lena Delta, Russia): A Multidisciplinary Approach, *Polar Geography*, 27, 277-319, 10.1080/789610225, 2003.
- 555 Schirrneister, L., Grosse, G., Schnelle, M., Fuchs, M., Krbetschek, M., Ulrich, M., Kunitsky, V., Grigoriev, M., Andreev, A., Kienast, F., Meyer, H., Babiy, O., Klimova, I., Bobrov, A., Wetterich, S., and Schwamborn, G.: Late Quaternary paleoenvironmental records from the western Lena Delta, Arctic Siberia, *Palaeogeography, Palaeoclimatology, Palaeoecology*, 299, 175-196, <https://doi.org/10.1016/j.palaeo.2010.10.045>, 2011.
- 560 Schirrneister, L., Froese, D., Tumskey, V., Grosse, G., and Wetterich, S.: Yedoma: Late Pleistocene ice-rich syngenetic permafrost of Beringia, in: *Encyclopedia of Quaternary Science*. 2nd edition, Elsevier, 542-552, 2013.
- Schneider, J., Grosse, G., and Wagner, D.: Land cover classification of tundra environments in the Arctic Lena Delta based on Landsat 7 ETM+ data and its application for upscaling of methane emissions, *Remote Sensing of Environment*, 113, 380-391, <https://doi.org/10.1016/j.rse.2008.10.013>, 2009.
- 565
- Schuur, E. A., Bockheim, J., Canadell, J. G., Euskirchen, E., Field, C. B., Goryachkin, S. V., Hagemann, S., Kuhry, P., Lafleur, P. M., and Lee, H.: Vulnerability of permafrost carbon to climate change: Implications for the global carbon cycle, *BioScience*, 58, 701-714, 2008.
- 570 Schuur, E. A. G., McGuire, A. D., Schädel, C., Grosse, G., Harden, J. W., Hayes, D. J., Hugelius, G., Koven, C. D., Kuhry, P., Lawrence, D. M., Natali, S. M., Olefeldt, D., Romanovsky, V. E., Schaefer, K., Turetsky, M. R., Treat, C. C., and Vonk, J. E.: Climate change and the permafrost carbon feedback, *Nature*, 520, 171, 10.1038/nature14338, 2015.
- Schwamborn, G., Rachold, V., and Grigoriev, M. N.: Late Quaternary sedimentation history of the Lena Delta, *Quaternary International*, 89, 119-134, [https://doi.org/10.1016/S1040-6182\(01\)00084-2](https://doi.org/10.1016/S1040-6182(01)00084-2), 2002.
- 575
- Shiklomanov, N. I., Streletskiy, D. A., Little, J. D., and Nelson, F. E.: Isotropic thaw subsidence in undisturbed permafrost landscapes, *Geophysical Research Letters*, 40, 6356-6361, 10.1002/2013gl058295, 2013.
- 580 Streletskiy, D. A., Shiklomanov, N. I., Little, J. D., Nelson, F. E., Brown, J., Nyland, K. E., and Klene, A. E.: Thaw Subsidence in Undisturbed Tundra Landscapes, Barrow, Alaska, 1962–2015, *Permafrost and Periglacial Processes*, 28, 566-572, 10.1002/ppp.1918, 2017.
- Swenson, S. C., Clark, M., Fan, Y., Lawrence, D. M., and Perket, J.: Representing Intrahillslope Lateral Subsurface Flow in the Community Land Model, *Journal of Advances in Modeling Earth Systems*, 11, 4044-4065, 10.1029/2019MS001833, 2019.
- 585



- Turetsky, M. R., Abbott, B. W., Jones, M. C., Anthony, K. W., Olefeldt, D., Schuur, E. A., Koven, C., McGuire, A. D., Grosse, G., and Kuhry, P.: Permafrost collapse is accelerating carbon release, *Nature*, 569, 32-34, 2019.
- 590 Ulrich, M., Grosse, G., Chabrillat, S., and Schirmermeister, L.: Spectral characterization of periglacial surfaces and geomorphological units in the Arctic Lena Delta using field spectrometry and remote sensing, *Remote Sensing of Environment*, 113, 1220-1235, <https://doi.org/10.1016/j.rse.2009.02.009>, 2009.
- West, J. J., and Plug, L. J.: Time-dependent morphology of thaw lakes and taliks in deep and shallow ground ice, *Journal of Geophysical Research: Earth Surface*, 113, 10.1029/2006jfe000696, 2008.
- 595 Westermann, S., Langer, M., Boike, J., Heikenfeld, M., Peter, M., Eitzelmüller, B., and Krinner, G.: Simulating the thermal regime and thaw processes of ice-rich permafrost ground with the land-surface model CryoGrid 3, *Geosci. Model Dev.*, 9, 523-546, 10.5194/gmd-9-523-2016, 2016.
- Zhang, T., Barry, R. G., Knowles, K., Heginbottom, J. A., and Brown, J.: Statistics and characteristics of permafrost and ground-ice distribution in the Northern Hemisphere, *Polar Geography*, 23, 600 132-154, 10.1080/10889379909377670, 1999.
- Zhang, T., Heginbottom, J. A., Barry, R. G., and Brown, J.: Further statistics on the distribution of permafrost and ground ice in the Northern Hemisphere, *Polar Geography*, 24, 126-131, 10.1080/10889370009377692, 2000.
- Zimov, S. A., Schuur, E. A., and Chapin, F. S.: Permafrost and the global carbon budget, *Science*, 312, 605 1612-1613, 2006.



Table 1: The excess ice initialization scenario in each of the three terraces (landunits) for the Lena River delta, as well as that for the single-landunit excess ice initialization case.

Depth (after adding ice)	Volumetric Ice content	Area weight
No excess ice terrain		
N/A	0%	24.6%
Holocene ground ice terrain		
0.9-9 m	65%	66.6%
Yedoma ice complex		
0.6-20 m	90%	8.8%
Average ice single-landunit case		
0.6-0.9 m	7.92%	100%
0.9-9 m	51.21%	100%
9-20 m	7.92%	100%

610



Table 2: The tiling scheme prescribing area weights of landunits for each CAPS class. The detailed CAPS classes are shown in Figure 2.

615

Overall Ground ice content for each CAPS point	Tiling scheme (area weights for each excess ice category)	Eligible CAPS types
5%	20% Low	clf; clf; slf; ilf; clr; dlr; slr; ilr
15%	20% Low; 22% Medium	cmf; dmf; smf; imf; dhr; shr; ihr
15%	20% Low; 14% High	chr
25%	20% Low; 22% Medium; 14% High	dhf; shf; ihf
25%	20% Low; 28% High	chf

Note: For each class, the first letter is for the permafrost extent, the second for the excess ice content, and the third for the terrain and overburden, following Brown et al. (2002).

Table 3: List of simulations conducted for this study.

Cases	Description
Single point cases for the Lena river delta	
Triple-landunit case	Applying the sub-grid representation of excess ice. Three natural vegetated landunit initialized.
Average ice single-landunit case	Not applying the sub-grid representation of excess ice. Only one natural vegetated landunit initialized. The grid-mean ice content for each soil layer in the only landunit is calculated by spatially averaging those in different landunits in the triple-landunit case.
Global simulation cases	
No ice case	Not adding any excess ground ice (the original CLM5 simulation).
Sub-grid ice case	Applying the sub-grid representation of excess ice. A tiling scheme helps to “translate” excess ice conditions in the CAPS data to fit what the CLM5 requires.
Grid-average ice case	Not applying the sub-grid representation of excess ice. The grid-mean ice content for each soil layer is calculated by spatially averaging those in different landunits in the sub-grid ice case.

620



625

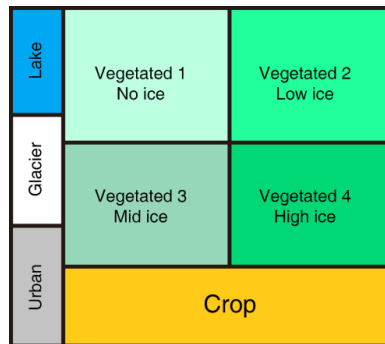
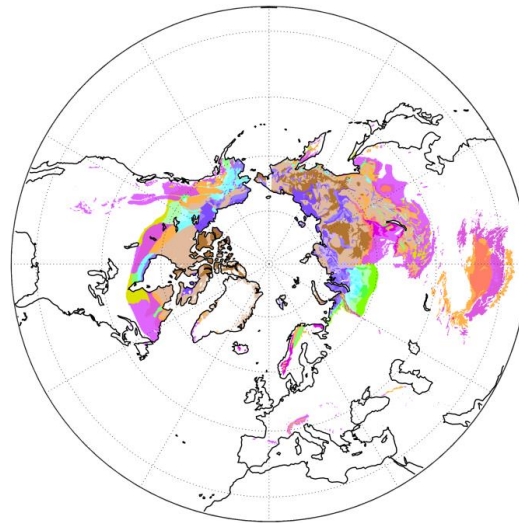


Figure 1: Modification of the CLM5 tiling hierarchy on the landunit level containing four natural vegetated landunits for different excess ice conditions.

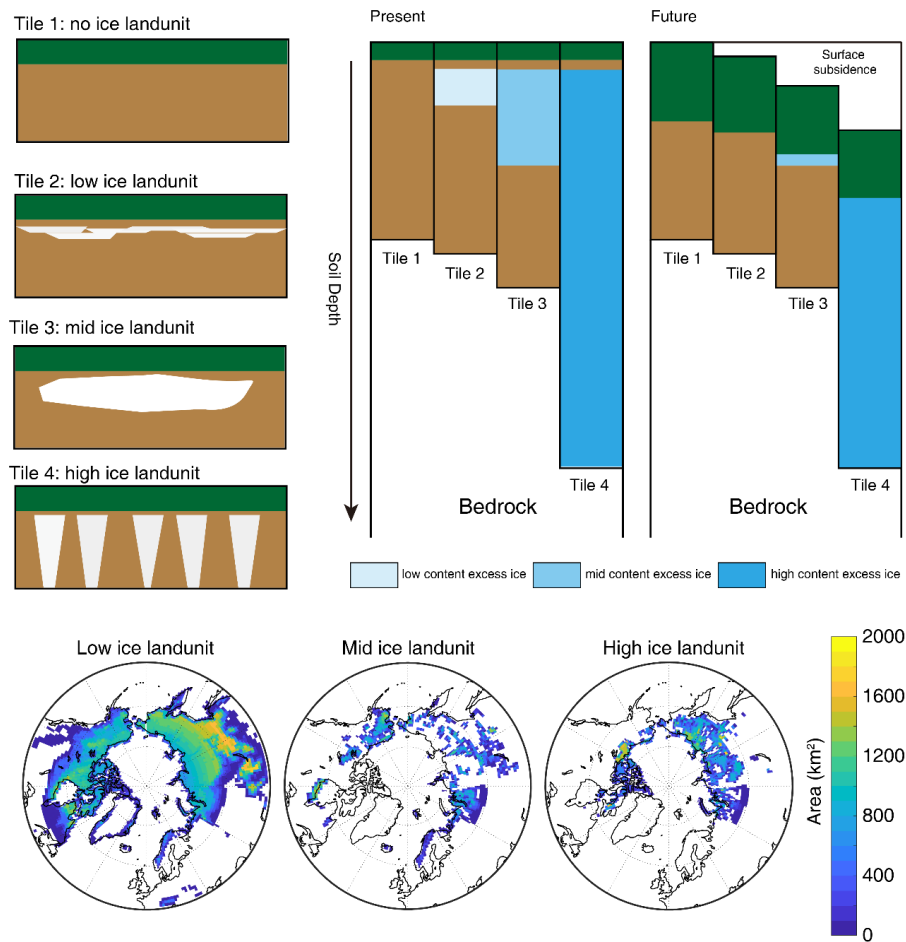


Permafrost area classification

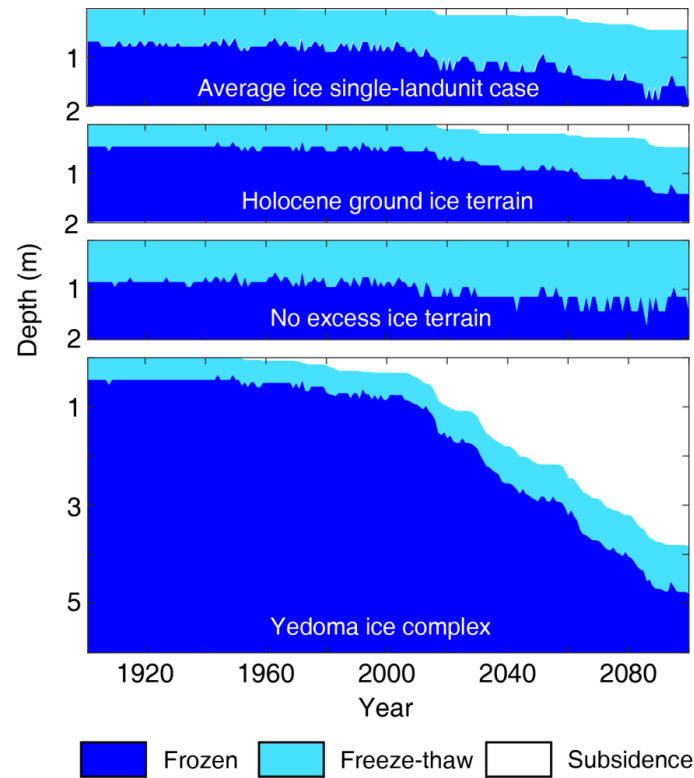
Permafrost Extent	Ground Ice Content (percent by volume)				
	Lowlands, highlands, and intra-and intermontane depressions			Mountains, highlands, ridges, and plateaus	
	25%	15%	5%	15%	5%
Continous (100%)	chf	cmf	clf	chr	clr
Discontinous (70%)	dhf	dmf	dlf	dhr	dhr
Sporadic (30%)	shf	smf	slf	shr	slr
Isolated (5%)	ihf	imf	ilf	ihr	ilr

* Letter code naming: The first letter is for the permafrost extent, second for the ground excess ice content, and the third for the terrain and overburden.

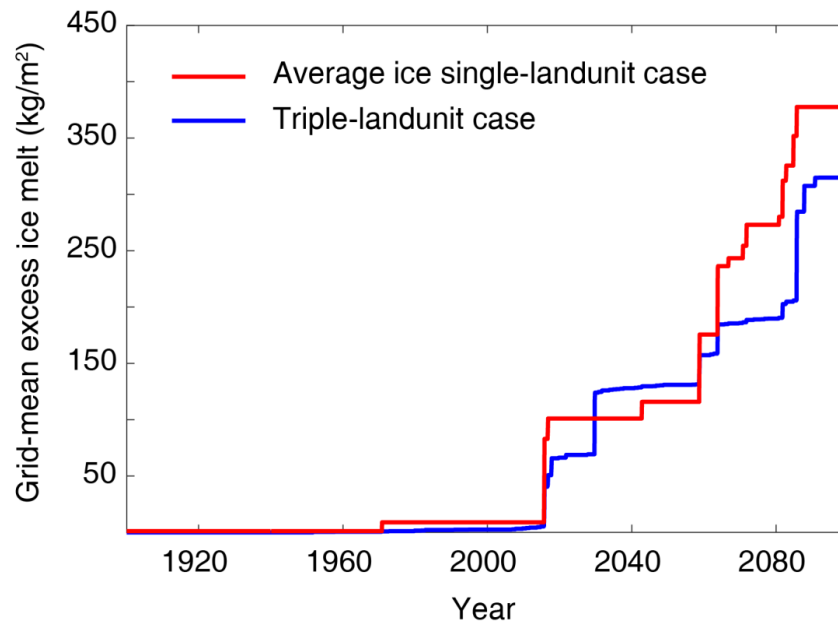
630 **Figure 2: Spatial distribution of excess ground ice in the Northern Hemisphere modified from Brown et al. (2002). Compared to the original data, permafrost extents and ground ice contents are converted to definite numbers (percentages) for model computation.**



635 **Figure 3.** Schematic representation of the sub-grid excess ice initialization scenario, and maps showing the area occupied by different excess ice landunits, i.e. the initial condition of excess ice in the global simulation.



640 **Figure 4.** Annual freeze-thaw state for the three terraces for the triple-landunit case, as well as for
the average ice single-landunit case.



645 **Figure 5. Grid-mean excess ice melt since 1900 for the single-point cases over the Lena river delta with and without the sub-grid excess ice initialization.**

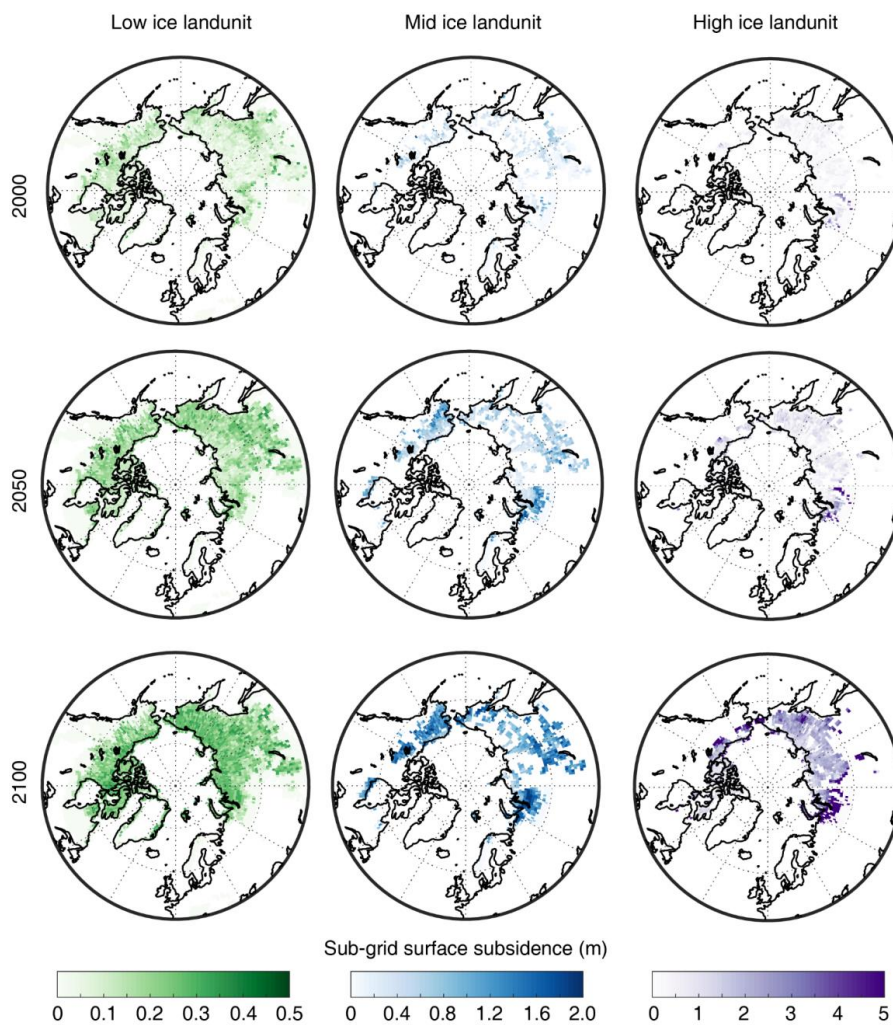
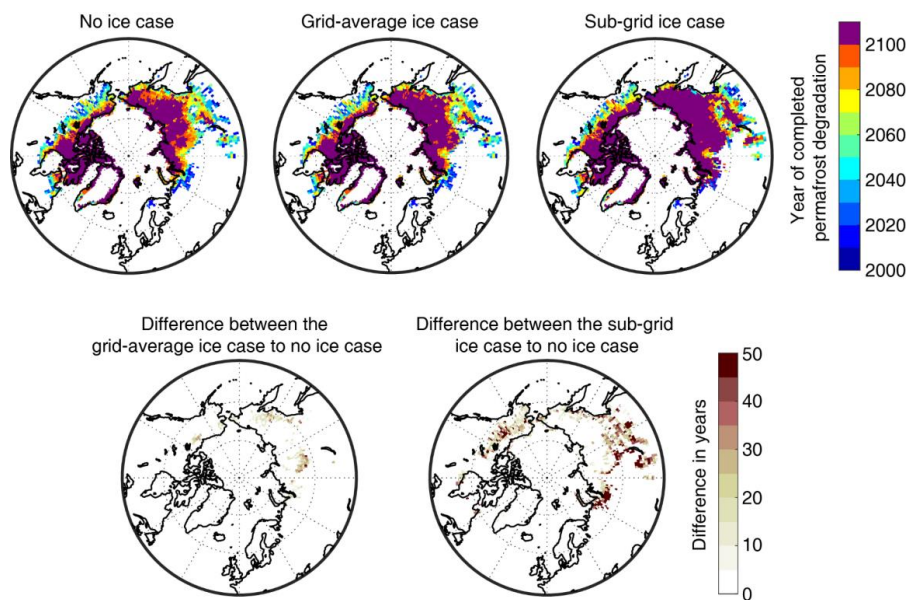


Figure 6. Maps showing sub-grid surface subsidence (m) in 2000, 2050, 2100 in the low, mid, and high excess ice landunits in the sub-grid ice case.

650



655 **Figure 7. Maps showing the year of completed permafrost degradation (upper set of three maps), as well as the differences between cases (lower set of two maps). The purple color indicates the existence of permafrost in these grid points by 2100. The difference in years is provided only for grid cell with completed permafrost degradation before 2100.**

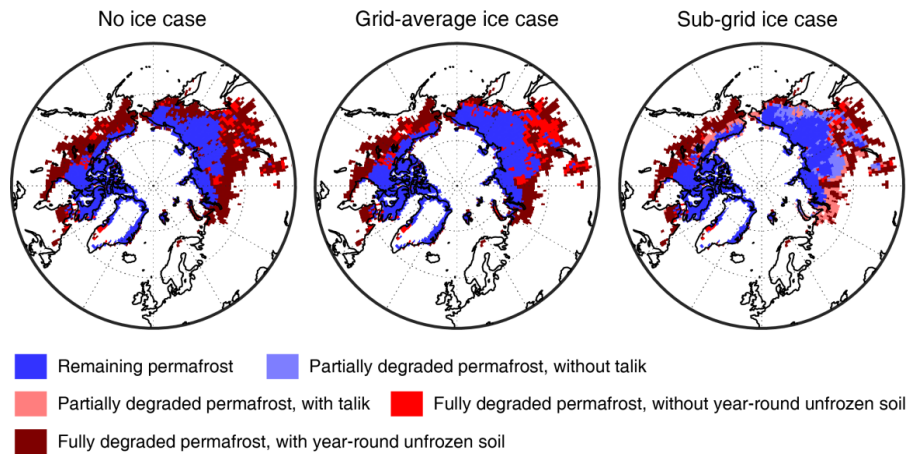


Figure 8. Maps of different stages of permafrost degradation diagnosed from the model output by the year 2100.

660

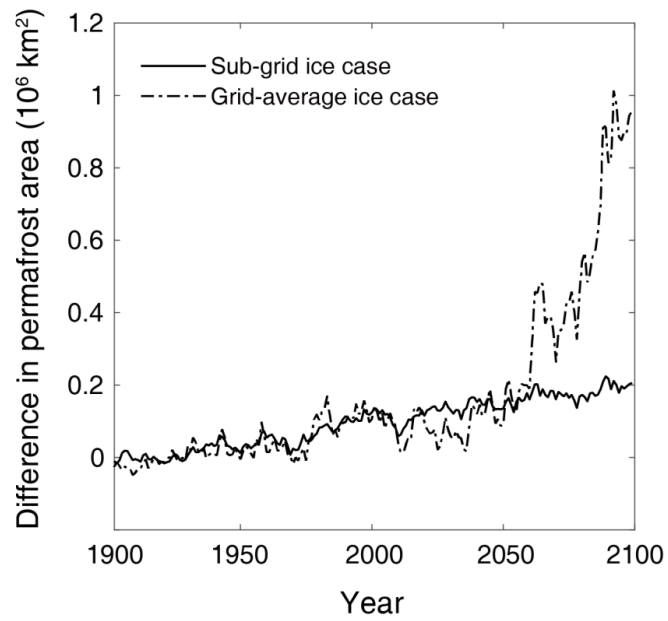


Figure 9. Difference in modeled permafrost area vs. time between the sub-grid ice case and no ice case, as well as between the grid-average ice case and no ice case.